# Large Bubble Rupture Sparks Fast Liquid Jet

Thomas Séon and Arnaud Antkowiak

*Institut Jean Le Rond d'Alembert, Université Pierre et Marie Curie and CNRS, UMR 7190, 4 Place Jussieu, F-75005 Paris, France*
(Received 12 December 2011; revised manuscript received 4 June 2012; published 2 July 2012)

This Letter presents the novel experimental observation of long and narrow jets shooting out in disconnecting large elongated bubbles. We investigate this phenomenon by carrying out experiments with various viscosities, surface tensions, densities and nozzle radii. We propose a universal scaling law for the jet velocity, which unexpectedly involves the bubble height to the power $3/2$. This anomalous exponent suggests an energy focusing phenomenon. We demonstrate experimentally that this focusing is purely gravity driven and independent of the pinch-off singularity.

Disrupting bubbles often exhibit violent jets during their ultimate fast out-of-equilibrium dynamics. Examples include bursting sea [1,2] or champagne bubbles [3], collapsing cavitation clouds [4] or submarine explosions [5] up to the astronomically sized buoyant bubble in elliptical galaxy M87 [6]. Among these violent jets, some are the signature of a finite-time singularity [7] occurring only for particular values of the control parameters [8], but in many cases, including those described here, jet formation is simply the result of a nonsingular relaxation process [9].

Before bursting, however, bubbles are not known to exhibit interface deformation as intense as the ones just depicted. Indeed, irrespective of their initial distortion [10] small bubbles gently relax toward robust equilibrium shapes in the form of spheres or oblate spheroids [11]. As regards the final form of larger bubbles, initial shape matters. According to their initial appearance, weakly deformed bubbles smoothly evolve either to spherical caps [12] or toroidal bubbles [13,14], as the ones typically expelled by dolphins or divers [15]. Much less is known about initially strongly deformed bubbles, as their dynamics and outcome have barely been studied. Such bubbles are yet commonplace in bubbling systems typically found in geophysics or industry (e.g., occurring in glassy [16] or metallic [17] melts). The primary aim of the present study is therefore to investigate the transient behavior of such large and highly deformed bubbles, which will prove to be as intense as bursting events.

In this Letter, we report a surprising violent jet dynamics following large bubble disconnection (Fig. 1) in a bubbling experiment. The thin and concentrated jet developing inside the bubble possibly gives rise to liquid projections shooting out way above the free surface. We analyze experimentally this phenomenon and we provide evidences of the role played by gravity in the jet formation.

Our experiments consist in releasing gas bubbles from a submerged orifice in a viscous liquid. The liquid is contained in a transparent tank taken sufficiently large (20 cm × 20 cm × 25 cm) to rule out confinement effects. The liquids used in this study include sugar cane syrup (Canadou) of viscosity $\mu = 110$ mPa · s and surface tension $\gamma = 90$ mN · m$^{-1}$ and three water-glycerol mixtures of viscosity $\mu = 140, 280, 420$ mPa · s and surface tension $\gamma = 65$ mN · m$^{-1}$. The height $h$ of fluid above the injector is typically kept in the range 5–10 cm. Air is fed through a nozzle of diameter 1.8 mm. Injection is controlled by a mass flow meter (Alicat Scientific) that provides a constant flow rate $Q$ by adjusting the air pressure. It allows us to achieve a wide range of airflows (from 0.01 to 10 $\ell$ · min$^{-1}$). The bubble and jet dynamics are analyzed through ultrafast imagery. To do so, the tank is back lit and images are obtained at 4000 frames per second using a digital high-speed camera (Photron SA-5).

Figure 1 illustrates a typical jetting event following the disconnection of a large gas bubble. Bubble pinch-off occurs on the first image and instantly a narrow, high-speed vertical jet shoots out inside the bubble. It is noteworthy that the bubble shape hardly deforms throughout the development of the jet, except near the fast recoiling conical rear. As the jet velocity is much higher than the bubble front velocity, the jet tip reaches the top of the bubble in a few milliseconds. Here, the jet is suddenly stopped as it collides with the bubble wall, but in other cases the jet literally perforates the bubble and makes headway in the bulk liquid.

In addition to the classical forces determining bubble volume [18], the detachment of the bubble is here potentially influenced by several other complex processes, including viscous stresses associated with the large scale convection pattern, gas pressure at the inlet, wake of the foregoing bubble, etc. However, we argue in the following that detachment is primarily due to the gravity-driven collapse of the bubble neck. We derive a simple model for the bubble formation, considering principally the expanding and contracting liquid motions induced by the bubble growth and seal process. The ambient liquid is mimicked by a finite set of slices in pure radial motion around a pressurized cavity [19,20]. Assuming a potential flow evolution, we can obtain an equation for the position of the free boundary $R(t)$ for each slice:

FIG. 1.    Time sequence of the jet developing inside a large bubble just after its release from a submerged nozzle. The large bubble pinches off at the first image and the back-to-equilibrium dynamics exhibits an intense and concentrated jet. The time lapse between the snapshots is $\Delta t = 3$ ms. The entire sequence lasts 18 ms and the bubble height, right after detachment, is $H = 4.22$ cm. The bubble front velocity is $V_{\text{front}} = 0.67$ m $\cdot$ s$^{-1}$ and the jet velocity is $V_{\text{jet}} = 2.69$ m $\cdot$ s$^{-1}$. The liquid viscosity is $\mu = 420$ mPa $\cdot$ s. The gas is injected through an injector of diameter $d = 1.8$ mm at an airflow rate of $Q = 4.4$ $\ell \cdot$ min$^{-1}$. The fluid height is $h = 10$ cm.

$$(R\ddot{R} + \dot{R}^2)\ln\frac{R}{R_\infty} + \frac{\lambda}{2}\dot{R}^2 = -\frac{P_{\text{bubble}}}{\rho} - gz + \frac{2\mu\dot{R} + \gamma}{\rho R}.$$

This is the 2D version of Rayleigh-Plesset equation describing the liquid motion around a hollow cylinder [21,22], with $\rho$ the liquid density, $g$ the gravity, $\lambda = 1 - R^2/R_\infty^2$ a confinement factor, $P_{\text{bubble}} = -\rho gH(t) + \gamma\kappa$ the bubble pressure, $\kappa = 2/R_{\text{front}}$ the front curvature, $R_\infty$ a distant cutoff, and $H(t) = V_{\text{front}}t$ and $z$ denoting, respectively, the height of the bubble and the local position of the slice. The bubble front is approximated by a frozen spherical cap of angle $2\theta$ rising at constant velocity. The cavity formation results from the air entrained behind it. The initialization procedure for each slice below this traveling bubble front simulates the deflection of fluid particles past it. At the trailing edge of the sphere portion, i.e., at the point $R(t) = R_{\text{front}}\sin\theta$ the following velocity is imposed: $\dot{R}(t) = dR/dt = V\cot\theta$. Figure 2 shows a typical face-to-face comparison between the experiment and the model. Remarkably, the overall detachment sequence is well captured even if the axial motions are disregarded [23]. This agreement between the experiment and a rough model containing as only driving force hydrostatic pressure constitutes a strong evidence that the seal mechanism is gravity driven.

We now turn to the jet formation *per se*, occurring right after the cavity closing. Figure 3(a) shows the experimental relation between the jet velocity $V_{\text{jet}}$ and the bubble height $H$, right after pinch-off instant. For all experiments, it was found from spatiotemporal diagram analysis that the velocity of the jet rapidly reaches a constant value after a transient regime. A clear trend appears from this figure: the jet velocity $V_{\text{jet}}$ increases with the bubble height $H$, consistently with a gravity-powered mechanism. Though exhibiting a visible tendency, the data are still quite spread out as for one value of the jet velocity correspond several bubble heights. To understand this spreading, let us examine the initial shape of some typical bubbles for a specific value $V_{\text{jet}} \simeq 2.7$ m $\cdot$ s$^{-1}$. In Fig. 3(a) are represented three bubbles, marked from 1 to 3, corresponding to the highlighted circles (bubble number 3 is the same as in Fig. 1). We observe that the three bubbles have a completely different shape, presenting a wide range of front curvature. Interestingly, the largest bubble (3) also bears the highest front curvature, while the smallest bubble (1) is the less curved. Yet in spite of these differences their jet velocities are the same. This geometrical competition between bubble height and front radius of curvature suggests a physical competition between an hydrostatic driving force and a capillary quenching effect: the main source of pressure difference between the liquid and the bubble is gravity, and capillarity tends to lessen this difference by pressurizing the bubble. In order to take both effects into account, we represent in Fig. 3(a) the jet velocity $V_{\text{jet}}$ versus the capillary corrected bubble height $H^\star = H - 2\gamma/\rho gR_{\text{front}}$. Upon using $H^\star$ instead of $H$, the three tracked experiments now get together as indicated by the arrows in Fig. 3(a). A similar gathering is observed for all experiments. This
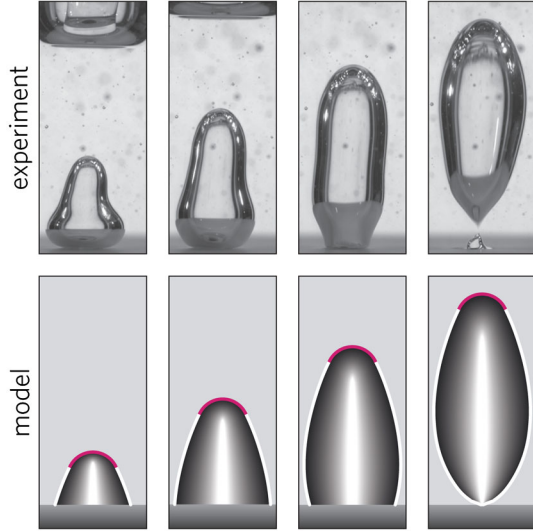
FIG. 2 (color online).  Comparison of experimental and simulated time sequences of bubble formation. In the model, the frozen spherical cap is materialized by a thick red line. The time lapse between each snapshot is $\Delta t = 11$ ms. The physical parameters are the air flow rate $Q = 3.80 \, \ell \cdot \text{min}^{-1}$, liquid viscosity $\mu = 280$ mPa $\cdot$ s, density $\rho = 1250$ kg $\cdot$ m$^{-3}$ and surface tension $\gamma = 65$ mN $\cdot$ m$^{-1}$. The parameters of the model $R_{\text{front}} = 4.18$ mm and $V_{\text{front}} = 0.785$ m $\cdot$ s$^{-1}$ are given by the experimental data. $R_\infty = 18.3$ mm and $\theta = 1.1$ rad are adjusted to the dynamics of the experiment. The slight shape dissimilarity is related to the absence of vertical motions in the theoretical model.



FIG. 3 (color online).   (a) Jet tip velocity ($V_{\text{jet}}$) as a function of heights: $H$ (open circle) height of the bubble after detachment (top axis) and $H^\star = H - 2\gamma/\rho g R_{\text{front}}$ (solid yellow circle) taking into account the capillary pressure term (bottom axis). The three bubbles presented in the bottom right corner labelled 1, 2 and 3 have the same jet velocity, but for a different height $H$ (highlighted in blue). When plotted with respect to $H^\star$, they all gather. The viscosity of the liquid is $\mu = 420$ mPa $\cdot$ s. (b) $V_{\text{jet}}$ as a function of $H^\star$ for four different viscosities $\mu$: 110 mPa $\cdot$ s (orange down triangle), 140 mPa $\cdot$ s (lavender square), 280 mPa $\cdot$ s (green triangle), 420 mPa $\cdot$ s (yellow circle). The surface tension and density are $\gamma = 65$ mN $\cdot$ m$^{-1}$ and $\rho = 1250$ kg $\cdot$ m$^{-3}$ except for the lowest viscosity (orange down triangle) for which $\gamma = 90$ mN $\cdot$ m$^{-1}$ and $\rho = 1350$ kg $\cdot$ m$^{-3}$. The injector diameter is $d = 1.8$ mm and the fluid height is $h = 10$ cm. The shaded area corresponds to discarded unsteady jets having a 'capillary Froude number' $V_{\text{jet}}/\sqrt{\gamma/\rho r}$, with $r$ the jet radius, below a typical value of 5: the feeding velocity $V_{\text{jet}}$ of these jets is too close to the retraction velocity $\sim\sqrt{\gamma/\rho r}$ hence their unsteadiness.

indicates the relevance of the parameter $H^\star$ and points to a pressure-driven mechanism for the jet formation, as is common in impact-driven [9] or gravity-driven jets [25].

The influence of viscosity $\mu$ and surface tension $\gamma$ in the development of the jet has been investigated as well by conducting similar experiments in various liquids. The results are summarized in Fig. 3(b). For each viscosity the same rise in jet velocity $V_{\text{jet}}$ with $H^\star$ is observed, albeit with a general shift to higher $H^\star$ with more viscous liquids.

Now taking the natural gravity-inertial velocity $\sqrt{gH^\star}$ and the nozzle radius $R_0$ as relevant scales of the problem, we nondimensionalized our results. The rescaled jet velocity or Froude number $\text{Fr} = V_{\text{jet}}/\sqrt{gH^\star}$ is plotted against the dimensionless height $H^\star/R_0$ in the bottom right inset of Fig. 4 for all viscosities, surface tensions and nozzle radii. Surprisingly enough, the six corresponding curves increase with respect to the dimensionless height. Actually we might have expected from a balance between buoyancy and inertia to observe a constant Froude number [25]. Rather we observe a linear variation of the Froude number with $H^\star/R_0$, identical for all sets of experiments. Moreover a shift to lower nondimensional velocities is noticeable as the viscosity is increased. This points to a functional dependence of the Froude number with $H^\star/R_0$ and the dimensionless viscosity as follows:
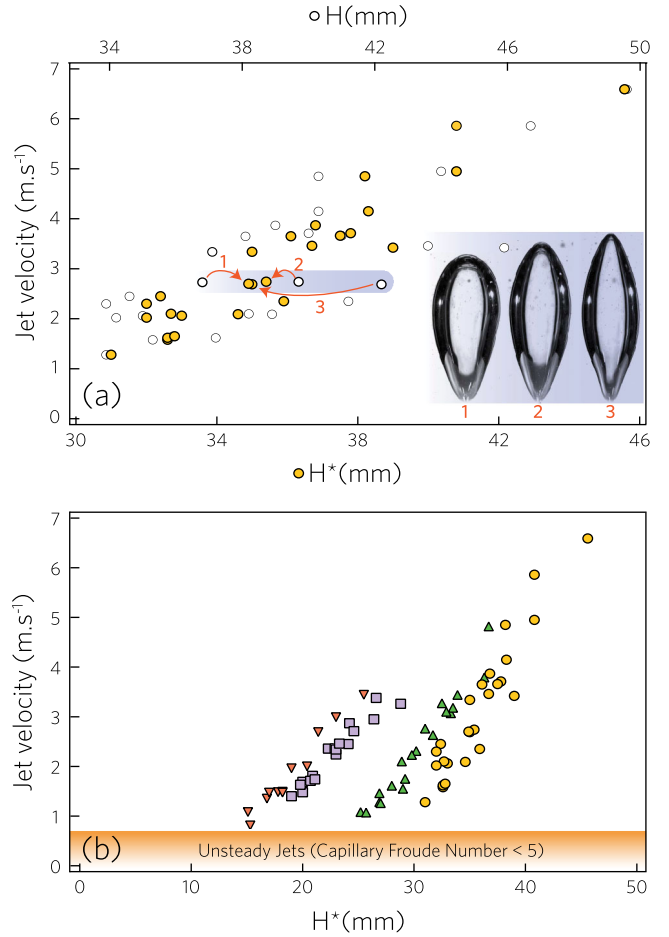
$$\frac{V_{\text{jet}}}{\sqrt{gH^\star}} = \alpha \frac{H^\star}{R_0} - \mathcal{F}\left(\frac{\mu}{\rho\sqrt{gH^\star}R_0}\right),$$

with $\alpha$ a nondimensional constant. Analysis of the experimental data reveals that the form of function $\mathcal{F}(x)$ is
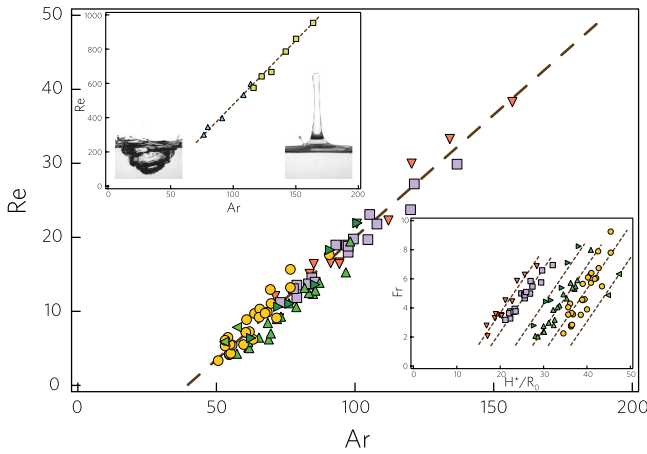
FIG. 4 (color online). Jet Reynolds number Re $= \rho V_{jet} R_0/\mu$ versus Archimedes number Ar $= \rho \sqrt{gH^\star} H^\star/\mu$ for different viscosities, surface tensions, densities and nozzle radii. The significance of the symbols is the same as in Fig. 3(b) and two series were added corresponding to two different injector diameters: 2.15 mm (dark green right triangle) and 1.19 mm (light green left triangle) with viscosity, surface tension and density, respectively, $\mu = 320$ mPa $\cdot$ s, $\gamma = 65$ mN $\cdot$ m$^{-1}$ and $\rho = 1250$ kg $\cdot$ m$^{-3}$. The equation of the oblique dashed line is Re $= \alpha$Ar $- \beta$, with $\alpha = 0.33$ and $\beta = 13$. The bottom right inset shows the Froude number Fr $= V_{jet}/\sqrt{gH^\star}$ versus the nondimensional bubble height $H^\star/R_0$. The lines act as eye guides and present the same slope $\alpha$. The top left inset presents the results of a different experiment where the jet is formed due to the gravitational collapse of a free surface hollow. By taking $H$ the depth of the cavity and $L$ the maximum cavity diameter as relevant scales, jet Reynolds number Re $= \rho V_{jet} L/\mu$ is plotted versus Archimedes number Ar $= \rho \sqrt{gH} H/\mu$ for two different viscosities $\mu$: 220 mPa $\cdot$ s (green square) and 426 mPa $\cdot$ s (blue triangle). The two snapshots display a typical cavity ($H = 5.61$ cm and $L = 12.6$ cm) and the resulting jet.

actually a linear function $\beta x$, with $\beta$ constant. This allows us to rewrite the preceding relation with a single identical offset for all viscosities:

$$\text{Re} = \alpha \text{Ar} - \beta,$$

where we have introduced the jet Reynolds number Re $= \rho V_{jet} R_0/\mu$ and Archimedes number Ar $= \rho \sqrt{gH^\star} H^\star/\mu$.

Figure 4 represents the relation between the jet Reynolds number and Archimedes number for all the conducted experiments. The collapse of the six series of experiments corresponding to five different viscosities, two surface tensions and densities and three different nozzle diameters is excellent. The relation between the jet velocity and the capillary corrected height of the bubble for the whole range of physical parameters is finally captured with the simple law Re $= \alpha$Ar $- \beta$. In systems exhibiting a balance between buoyancy and inertia, the potential volume energy $\sim \rho g H$ is converted into kinetic volume energy $\sim \rho V^2$ and the velocity typically scales as $H^{1/2}$: large Taylor bubbles

in tubes [12], gravity waves in shallow fluid layers [26], inertial gravity current [27]. Surprisingly, the here obtained scaling law shows a dependence of the jet velocity $V_{jet}$ with $H^{\star 3/2}$ rather than $H^{\star 1/2}$. This anomalous exponent suggests an energy focusing phenomenon whose source is now discussed.

Does the pinch-off singularity play a role in this focusing? In order to investigate the role of detachment, we have designed and carried out a new model experiment, free of pinch-off. This experiment consists in blowing air over a free liquid surface so as to form a depression, mimicking the conical rear of the bubble. Upon the collapse of this hollow, a gravity-driven jet develops (see snapshots in Fig. 4). But there again, the same scaling for the jet velocity with $H^{3/2}$ is observed (top left inset). Note also that, in sharp contrast with singular focusing behaviors [7], the cavity reversal observed here is not unlike the shell eversion process in that jet eruption or curvature reversal happens before collapse. These rule out both pinch-off [28–30] and curvature singularities [7] in the observed energy focusing and demonstrate that it is merely a signature of the gravitational cavity collapse.

Finally, in this Letter we have focused on the jet development before its collision with the bubble front. An open remaining question is whether the jet could have a sufficient energy to perforate the bubble and reach the free surface. In our experiments we observed that strong liquid projections can appear above the free surface for large airflow rate. We are currently investigating the highly unclear link between the jet presented here and these liquid projections.

[1] D. C. Blanchard, *From Raindrops to Volcanoes* (Doubleday, New York, 1967).
[2] L. Duchemin, S. Popinet, C. Josserand, and S. Zaleski, Phys. Fluids **14**, 3000 (2002).
[3] G. Liger-Belair, C. Cilindre, R. D. Gougeon, M. Lucio, I. Gebefügi, P. Jeandet, and P. Schmitt-Kopplin, Proc. Natl. Acad. Sci. U.S.A. **106**, 16 545 (2009).
[4] T. B. Benjamin and A. T. Ellis, Phil. Trans. R. Soc. A **260**, 221 (1966).
[5] M. Lavrentiev and B. Chabat, *Effets Hydrodynamiques et Modèles Mathématiques* (Éditions MIR, Moscow, 1980).
[6] E. Churazov, M. Brüggen, C. R. Kaiser, H. Böhringer, and W. Forman, Astrophys. J. **554**, 261 (2001).
[7] B. W. Zeff, B. Kleber, J. Fineberg, and D. P. Lathrop, Nature (London) **403**, 401 (2000).
[8] M. P. Brenner, Nature (London) **403**, 377 (2000).

[9] A. Antkowiak, N. Bremond, S. Le Dizès, and E. Villermaux, J. Fluid Mech. **577**, 241 (2007).

[10] B. Yang, A. Prosperetti, and S. Takagi, Phys. Fluids **15**, 2640 (2003).

[11] J. Magnaudet and I. Eames, Annu. Rev. Fluid Mech. **32**, 659 (2000).

[12] R. M. Davies and G. Taylor, Proc. R. Soc. A **200**, 375 (1950).

[13] J. K. Walters and J. F. Davidson, J. Fluid Mech. **17**, 321 (1963).

[14] T. Bonometti and J. Magnaudet, Phys. Fluids **18**, 052102 (2006).

[15] K. Marten, K. Shariff, S. Psarakos, and D. J. White, Sci. Am. **275**, 82 (1996).

[16] J. E. Shelby, *Introduction to Glass Science and Technology* (The Royal Society of Chemistry, London, 2005), 2nd ed.

[17] A.-G. Guézennec, J.-C. Huber, F. Patisson, P. Sessiecq, J.-P. Birat, and D. Ablitzer, Powder Technol. **157**, 2 (2005).

[18] R. Clift, J. R. Grace, and M. E. Weber, *Bubbles, Drops, and Particles* (Academic, London, 1978).

[19] D. Lohse, R. Bergmann, R. Mikkelsen, C. Zeilstra, D. van der Meer, M. Versluis, K. van der Weele, M. van der Hoef, and H. Kuipers, Phys. Rev. Lett. **93**, 198003 (2004).

[20] V. Duclaux, F. Caillé, C. Duez, C. Ybert, L. Bocquet, and C. Clanet, J. Fluid Mech. **591**, 1 (2007).

[21] H. N. Oguz and A. Prosperetti, J. Fluid Mech. **257**, 111 (1993).

[22] J. C. Burton, R. Waldrep, and P. Taborek, Phys. Rev. Lett. **94**, 184502 (2005).

[23] In the context of the deep seal of a transient impact-generated cavity, the 2D Rayleigh-Plesset model is also in excellent agreement with the experiments, even if the vertical motions are neglected [24]. This suggests that the relevant mechanism for the pinch-off is radial in essence.

[24] R. Bergmann, D. Van Der Meer, S. Gekle, A. Van Der Bos, and D. Lohse, J. Fluid Mech. **633**, 381 (2009).

[25] R. Bergmann, E. Dejong, J.-B. Choimet, D. Van Der Meer, and D. Lohse, J. Fluid Mech. **600**, 19 (2008).

[26] G. B. Whitham, *Linear and Nonlinear Waves* (Wiley, New York, 1974).

[27] J. E. Simpson, *Gravity Currents in the Environment and the Laboratory* (Cambridge University Press, Cambridge, England, 1997), 2nd ed.

[28] R. Bolanos-Jimenez, A. Sevilla, C. Martinez-Bazan, and J. M. Gordillo, Phys. Fluids **20**, 112104 (2008).

[29] D. Bartolo, C. Josserand, and D. Bonn, Phys. Rev. Lett. **96**, 124501 (2006).

[30] S. Gekle and J. M. Gordillo, J. Fluid Mech. **663**, 293 (2010).